Energy Conversion and Management 250 (2021) 114891

Contents lists available at ScienceDirect

Energy Conversion and Management

journal homepage: www.elsevier.com/locate/enconman

Mismatch losses in a PV system due to shortened strings

Ryan M. Smith [a,*], Manjunath Matam [b], Hubert Seigneur [b]

[a] Pordis LLC, Austin, TX, United States
[b] University of Central Florida, Orlando, FL, United States

ARTICLE INFO

Keywords:
Photovoltaic module
String
Mismatch
MPP
Reverse current
Modeling

ABSTRACT

Numerous events may require intentional removal of one or more photovoltaic modules from a string, shortening the length of the string relative to others within the array, resulting in a str ing length mismatch. The impact of such a mismatch is not well understood either in measurable operational effects (voltage, current, power) or in the potential effects on long-term module health. It is impractical to solely approach this problem experimentally due to the size and complexity of arrays that may experience string length shortening. This work presents simulations, validated through limited field experiments on a two string array, providing a basis from which more complex arrays and scenarios may be explored. Refinement of the simulation achieves an overall error in I_{MPP} for the nominal (S_1) and test strings (S_2) between the simulation and experimental values, through all test conditions, of $+0.35 \pm 1.46\%$ and $-0.36 \pm 1.58\%$ respectively. Shortening one of two strings by one module results in a power loss greater than the power contribution of the module alone (1.29 module equivalents); the impact increases through the maximum test case of a six module mismatch with a power loss equivalent to more than 11 modules. The impact of using string-end blocking diodes is presented with an emphasis at the array maximum power point and at open circuit. Implications are discussed for arrays of higher complexity.

1. Introduction

Solar is now less expensive than traditional forms of energy production in many states and countries. Many nations, states, and utilities have set ambitious targets to install tens to hundreds of gigawatts of photovoltaic (PV) generation in the next five to ten years [1]. At the same time, utility projections regarding the levelized cost of energy (LCOE) must be consistent with renewable generation targets to remain a viable alternative in their portfolios [2]. Major sources of energy loss in a PV system, other than the inherent unavoidable conversion/ transmission losses, consist of under-performance due to faults, prolonged PV system unavailability, and mismatch losses [3–5]. Mismatch conditions alone were reported to cause up to 20 to 25% reduction in the output of the PV system [6]. The mismatch can occur in the module current because modules are connected in a series, or in the string voltage because strings are connected in parallel.

Many operational factors can force the PV array to operate under mismatch conditions, resulting in medium to large power losses, and therefore must be avoided or mitigated [7–18]. Mismatch conditions can occur from manufacturing tolerances, although typically less than 1% nowadays [19] down from 4–7% [20], or from combining modules of varying models, manufacturers, and technologies. In [21], a mismatch study of strings consisting of different technologies was conducted. The authors recommend against connecting different technology modules in the same string, however, connecting same current rating modules in series, and connecting same voltage rating modules in parallel is permitted. Discrepancies in the PV system installation such as module tilt angles and orientation can cause mismatch conditions. Environmental conditions such as shading, soiling, snow, or temperature gradient [20] can also result in mismatch conditions. In [22], the impact of partial shading on different PV module technology arrays has been investigated through simulation studies. Different technology PV arrays showed different power losses when the mismatched PV modules are present in the string: thin-film technology PV array experienced 0.7% power losses, multi-crystalline technology PV array experienced 0.6% power losses, and the mono-crystalline PV array experienced 0.4% power losses. In [23], shading induced mismatch losses in bifacial PV systems and their impact on annual yields were studied and found to be highly dependent on factors such as row to row spacing, position within the string, and non-uniform albedo. Mismatch conditions can also be caused by non-electrical PV faults, such as non-uniform module aging, cell cracks, cell interconnect failures, encapsulant browning, hot spots,

* Corresponding author.
E-mail address: ryan.smith@pordis.com (R.M. Smith).

https://doi.org/10.1016/j.enconman.2021.114891
Received 14 May 2021; Received in revised form 24 September 2021; Accepted 15 October 2021

voltage drop on the home run lines to the inverters, faults in tracker systems, and so on. In [24], PID impacted 17 modules of a negatively grounded monocrystalline silicon string in a 20 MW PV field were tested indoors under standard test conditions. Results revealed a 1.9% mismatch loss in the string caused by non-uniform degradation of the modules; those close to the negative terminal degraded faster compared to the positive terminal. Bypass diode failure-based voltage mismatch conditions have been reported in [25,26]. These factors can progress slowly over time or happen suddenly, leading to significant power losses, as in the case of PV electrical faults such as line to line faults or line to ground faults.

Another key operational factor that can lead to severe mismatch conditions is shortened strings, our focus in this publication. When modules are removed or go missing and a replacement module is not available, one practice is to bypass the removed module(s), leaving shortened strings [27]. Solar plant owners have a limited amount of extra identical modules available in storage to replace missing modules. Solar panel manufacturers are constantly improving their technology, rendering any given model obsolete within a few years; as a result, they are not able to provide extra identical modules. String shortening can happen due the annual removal and shipping of PV modules to indoor labs for performance testing in order to assess annual degradation rates in each plant, resulting in many modules missing over several weeks. Additionally, modules are removed from time to time for routine maintenance and fault diagnosis activity [28]. String shortening may also happen due to theft or after a natural disaster such as hail, high wind, flooding, lightening strikes, or fire when modules are not immediately replaced due to challenges with availability, insurance, or warranty claims[29]. Because the industry is experiencing rapid growth and increased frequency and impact of natural disasters due to climate change, string shortening might become more widespread, potentially leading to significant mismatch losses at the utility level. In smaller systems, such as residential and some commercial rooftop applications, available space may not permit uniformly equal length strings, so the system may have shortened strings by design. It is important to understand the implications of mismatched string lengths on array performance.

The few mismatch studies reported in the literature have briefly investigated the impact of shortened strings on overall PV plant output through simulation studies. However, they did not perform experimental investigation, analyze reverse current flow in the shortened strings, determine the impact of string-end blocking diodes on string output, or determine the impact of mismatch on module temperature. In [30], a simulation study was conducted to understand the mismatch losses caused by the integration of PV modules from varying manufacturers or models and various installation configurations. Although they compare mismatch losses due to missing modules with losses due to replacement modules of a different manufacturer or model using simulations, they do not provide the experimental validation or details about damage mechanisms or other practical implications for PV systems operating under such conditions. In [31], simulation studies based on the one-diode model (ODM) and an IV curve fitting model have quantified power losses involving combinations of unequal length strings. However, actual operating conditions were not taken into account. Beyond the need to understand operational impacts, the impact of a string length mismatch on the nominal and shortened strings is not fully studied. In [32], the authors remind us that current electrical codes and standards for PV systems lack detailed guidance regarding circuit mismatch, over or reverse current protection and unbalanced operational conditions in large PV systems because experimental work in this field is expensive and limited by hardware and environmental resources. Furthermore, they showed that fault reverse currents are determined by fault types, fault location, and the action of the inverter. Although some studies have reported on experimental reverse current flow and the impact of blocking diodes, it was done in connection with faults other than shortened strings [32,6].

To address the limitations of previous work, this paper performs shortened string mismatch analysis through both simulation and experiment. The objective is to understand the impact of shortened strings on the overall system output and reverse current flow. This work presents an LTSpice based mismatch simulation model and the experimental validation results under various mismatch conditions. Simulation and experimental studies were conducted under two cases: with blocking diodes and without blocking diodes. The majority of PV plants do not use blocking diodes. When PV modules are removed and a string length mismatch is created, the blocking diodes case helps to understand the pros and cons of integrating blocking diodes into the shortened strings to prevent reverse current flow. This paper is organized as follows: Section 2 presents the PV system configuration used in the simulation and experimental studies; Section 3 discusses simulation and experimental results obtained under various mismatch conditions as they pertain to model creation and validation; Section 4 discusses the simulation and experimental results; and Section 5 presents conclusions.

2. PV system configuration

The photovoltaic system configuration used in the simulation and experimental study consists of two identical strings of twelve Jinko Eagle 60 polycrystalline silicon modules per string, in parallel, connected to an SMA grid-tied inverter with a single utilized maximum power point tracker. Key manufacturer specification sheet parameters are provided in Table 1 [33].

The PV array is shown in Fig. 1 and schematically in Fig. 2. String S_1 is the reference string, which remains unchanged throughout the study. A portion of the modules within string S_2 are electrically disconnected from the string to shorten its module count and create mismatch conditions. Between zero and six modules are removed from S_2 throughout the study. Strings of equal module count is termed the “nominal” condition with mismatched length strings termed “1-module shortened” through “6-module shortened” in reference to the difference in module count between S_1 and S_2. A portion of this work is interested in discerning behavior differences between arrays with and without string-level blocking diodes both at the maximum power point and at open circuit, a condition which exists when the inverter is offline or disconnected from the AC grid.

3. Model creation and validation

Simulation provides an efficient means to elucidate the behavior of an array of equal- and unequal-length parallel strings. A simple simulation framework provides sufficient detail to understand the behavior of arrays of varying unequal length strings under real-world field conditions without requiring specific knowledge of the exact model parameters typically associated with these types of simulations. A model built of simple elements in a widely available software package, LTSpice [34], is effective in simulating the behavior of complex arrays. A simplified flowchart of the model optimization and simulation process is shown in Fig. 3. Section 3.1 introduces a simple model and procedure for simulation of arrays under real-world conditions. Section 3.2 describes field studies of a grid-connected, 6.2kW two-string test array under

Table 1
Jinko Eagle 60 270W polycrystalline silicon module STC parameters from the manufacturer specification sheet [33].

Model	JKM270PP-60
P_{max}	270Wp
V_{mpp}	31.7V
I_{mpp}	8.52A
V_{oc}	38.8V
I_{sc}	9.09A
Series Fuse	15A

Fig. 1. The two string, grid-tied 6.2kW experiment array at the UCF FSEC test field in Cocoa, Florida.

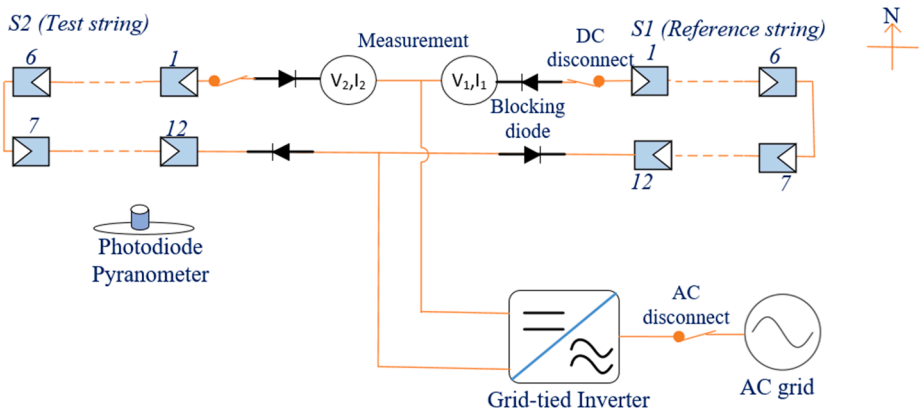

Fig. 2. Schematic of the two string, grid-tied 6.2kW experiment array at the UCF FSEC test field in Cocoa, Florida.

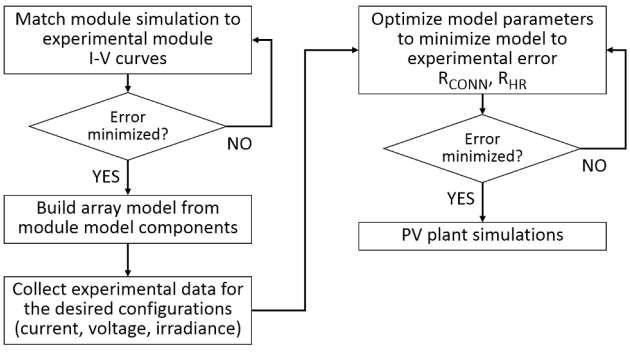

Fig. 3. A simplified flowchart of the developed model creation, optimization, and simulation processes..

multiple sets of conditions. Field data validates the effectiveness of the model in predicting real-world system behavior under inverter MPP tracking. Finally, Section 3.3 reviews simulation and experimental results under open-circuit conditions.

3.1. Photovoltaic module simulation model and parameter extraction

String-level simulations are built from the simplest constituent model elements of a photovoltaic string, the module. A single diode model of the module, described schematically in Fig. 4, is built in the LTSpice software package. By default, LTSpice elements are treated as thermally static at 27°C. However, to compare the simulation results against experimental field data, simulations must be performed at readily experienced operating conditions; field measurement raw data provides regular conditions of 50°C and 800W/m^2 for the test site. Although cell temperatures will differ from this average value due to natural environmental variation, the average value is a reasonable simplification to achieve the goals of this work.

Adjustment of the PV module response to temperature requires an explicit understanding of the change in equivalent circuit parameters with temperature. Extraction of temperature- and irradiance-dependent parameters is performed using the technique described by Cubas [35]. Module manufacturer specification sheet parameters at STC conditions

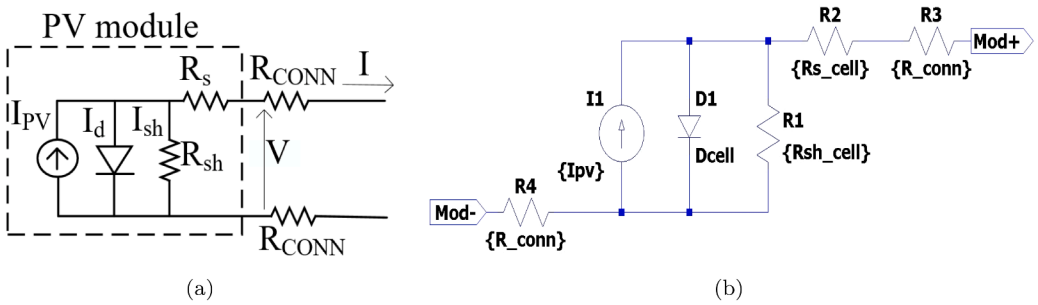

Fig. 4. (a) Single diode equivalent circuit, and (b) LTSpice model of the Jinko Eagle 60 270W polycrystalline silicon module.

of 1000W/m^2, 25°C, and AM1.5 spectrum, Table 1, are used to obtain decoupled explicit equations for the equivalent circuit parameters, Eqs. (1)–(5). Calculated terms for each equation are listed in Table 2. G_R is the reference irradiance of 1000W/m^2; T_R is the reference temperature of 25°C.

$$\Delta T = T - T_R \tag{1}$$

$$R_s(T) = A + B\Delta T + C\Delta T^2 + D\Delta T^3 \tag{2}$$

$$R_{sh}(T) = \frac{1}{A + B\Delta T + C\Delta T^2 + D\Delta T^3} \tag{3}$$

$$I_0(T) = exp(A + B\Delta T + C\Delta T^2 + D\Delta T^3) \tag{4}$$

$$I_{PV}(T, G) = (A + B\Delta T + C\Delta T^2 + D\Delta T^3)\frac{G}{G_R} \tag{5}$$

In addition to the temperature- and irradiance-dependent parameters (R_s, R_{sh}, I_0 and I_{PV}), the simulation model is augmented with additional elements to reflect actual system installation. Two fixed resistance elements (R_{CONN}, measured sample average of 0.013Ω) add the resistive contribution of the module's integrated cables and connectors to the module-level model, shown schematically in Fig. 4. As implemented, the module-level model simulates the module within reasonable agreement to the specification sheet NOCT values for voltage parameters, but underestimates current parameters: I_{SC} (-1.1%), V_{OC} (+0.23%), I_{MPP} (-2.9%), V_{MPP} (-0.01%), maximum power P_{MAX} (-2.9%), and fill factor FF (-2.06%), calculated from other parameters). The error in calculated fill factor is attributed to the underestimate of I_{SC} and I_{MPP}.

3.2. 6.2kW PV plant simulation and model validation at MPP

In order to simulate the potential impact of string mismatch in arrays, it is necessary to validate that the simulation predictions for the maximum power point have a basis in reality. The simulation is therefore expanded beyond the module level to match the configuration of the field test array. Experiments where the length of the test string, S_2, is shortened from the nominal length of twelve modules to a length of six modules provides data for conducting an analysis against the simulations.

Table 2
Decoupled explicit equation terms for equivalent circuit parameters.

Parameter	Term	Value
R_s	A	0.25190297
	B	−0.00136633689770084
	C	9.07057495906687E-07
	D	−1.01318992738693E-09
R_{sh}	A	0.00271753
	B	−4.80138188416594E-05
	C	6.95196392972283E-09
	D	−1.2298554099918E-11
I_0	A	−20.6851569221229
	B	0.0769524637863597
	C	−0.000256325726524487
	D	7.29114480609597E-07
I_{PV}	A	9.0962226194945
	B	−0.0001436980956205
	C	6.34358452572244E-07
	D	−5.00770373088239E-10

The array-level model, Fig. 5, consists of two parallel strings of twelve module elements each. Home run cable and connector resistance is added at the end of each string (R_{HR}) along with blocking diodes, D1 and D2, used for the V_{OC} portion of this study. The initial value of R_{HR} is fixed at the same value as R_{CONN} of 0.013Ω; refinement of R_{HR} is discussed later in this section. Throughout the model, a multitude of resistive elements act as nominally zero- or infinite-ohm resistances and enable programmatic reconfiguration of the array model into specific configurations. Note that element C1 is included to improve simulation computation success by reducing the chance of the simulation hanging at an unsolvable state; this small 10 picofarad capacitance has a minimal impact on result of the simulations. With this model, one string (S_1) remains at the nominal length of twelve modules while the test string (S_2) is systematically shortened from twelve modules to six modules, both with and without string-level blocking diodes. The expectation is that as the strings are increasingly mismatched, the maximum power point of the array will decrease in voltage and current, with the most significant changes to V_{MPP}. Blocking diodes prevent the shortened string from operating under reverse current above its V_{OC}. In the absence of blocking diodes, the shortened string will experience reverse current between its V_{OC} and the V_{OC} of the mismatch array.

An example simulation with blocking diodes is shown in Fig. 6 for the condition of a 3-module mismatch between S_1 and S_2. The upper portion of the figure indicates the nominal array IV curve (solid yellow; for reference), the individual string IV curves for the nominal (solid black, S_1) and shortened (dashed blue, S_2) strings, and the mismatch array IV curve (dashed red). Maximum power points for each IV curve are indicated. The V_{MPP} of the array decreases due to the mismatch (yellow diamond to red dot). Given the mismatch array maximum power point, the nominal string is expected to operate at a higher current than the shortened string. This is shown in the lower portion of the figure; the expected operating point of each string is indicated.

A simulation without blocking diodes is shown in Fig. 7 for the condition of a 3-module mismatch between S_1 and S_2. The scale is the same as that of Fig. 6. The upper portion of the figure also indicates the nominal array IV curve (solid yellow; for reference), the individual string IV curves for the nominal (solid black, S_1) and shortened (dashed blue, S_2) strings, and the mismatch array IV curve (dashed red). Maximum power points for each IV curve are indicated. Similar to the simulation with blocking diodes, the V_{MPP} of the array decreases due to the mismatch (yellow diamond to red dot) and is of a comparable value. Given the mismatch array maximum power point, the nominal string is also expected to operate at a higher current than the shortened string.

Initial comparisons of the nominal array-level simulation, where both strings are of nominal length, against nominal experimental data, shows differences that are not additive of the differences seen at the

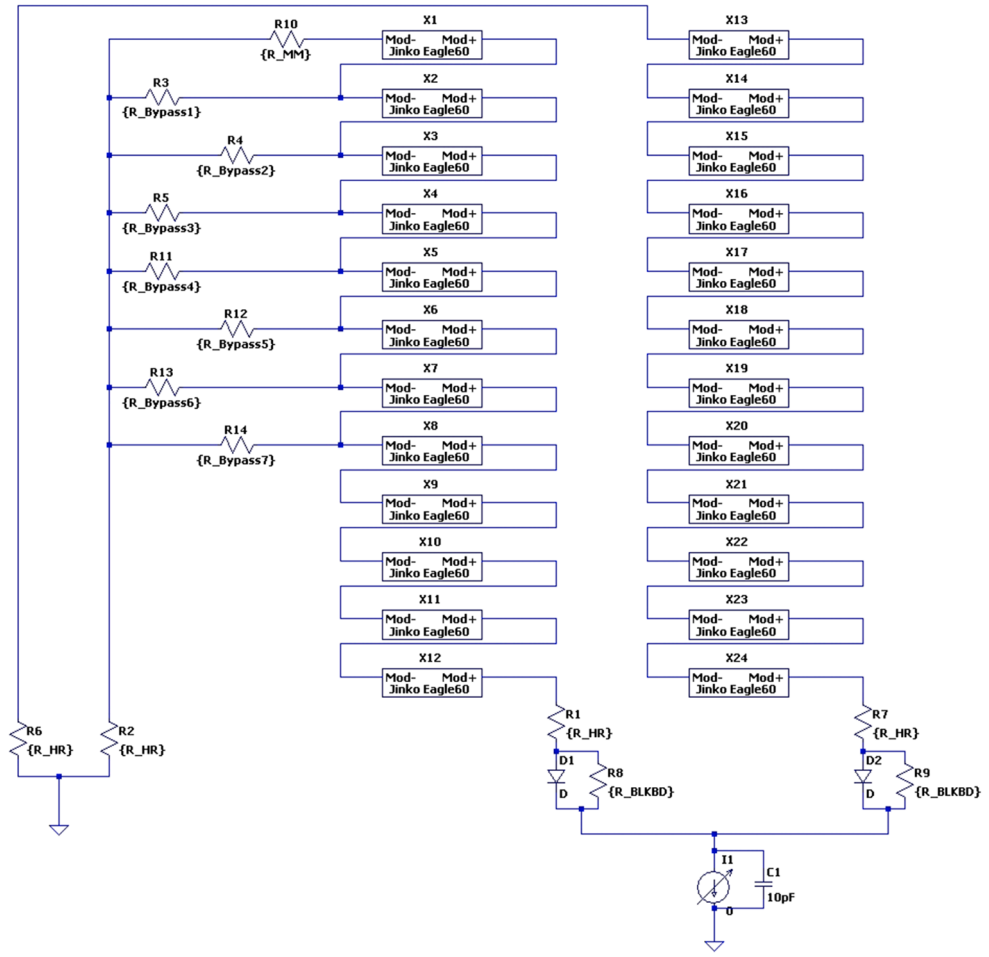

Fig. 5. LTSpice model of the two string, grid-tied 6.2kW experiment array at the UCF FSEC test field in Cocoa, Florida.

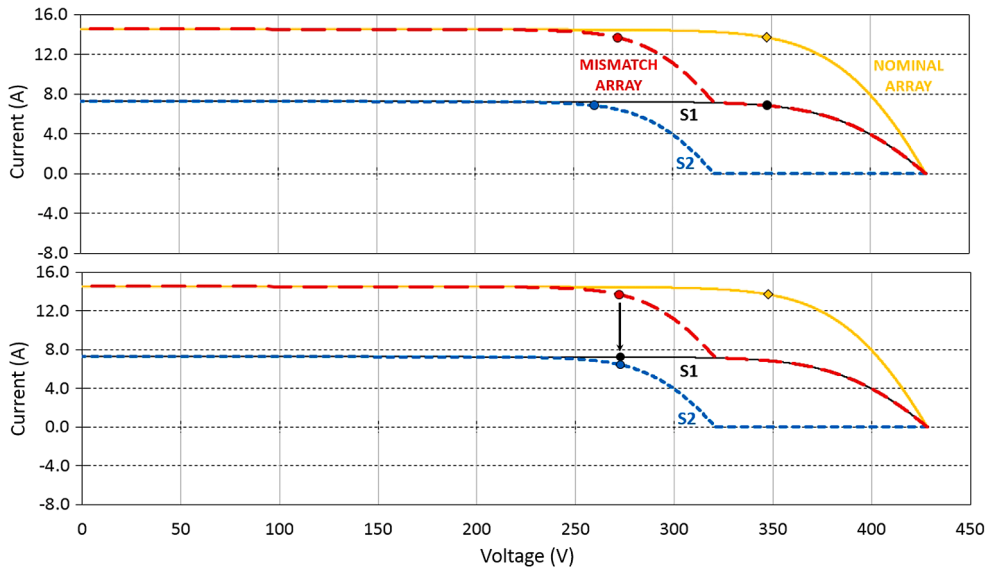

Fig. 6. Simulation of a 3-module mismatch with blocking diodes. a) the upper portion indicates the nominal array IV curve (solid yellow; for reference), the individual string IV curves for the nominal (solid black, S_1) and shortened (dashed blue, S_2) strings, and the mismatch array IV curve (dashed red). Maximum power points for each IV curve are indicated. b) the lower portion indicates the expected operating point of each string given the mismatch array maximum power point.

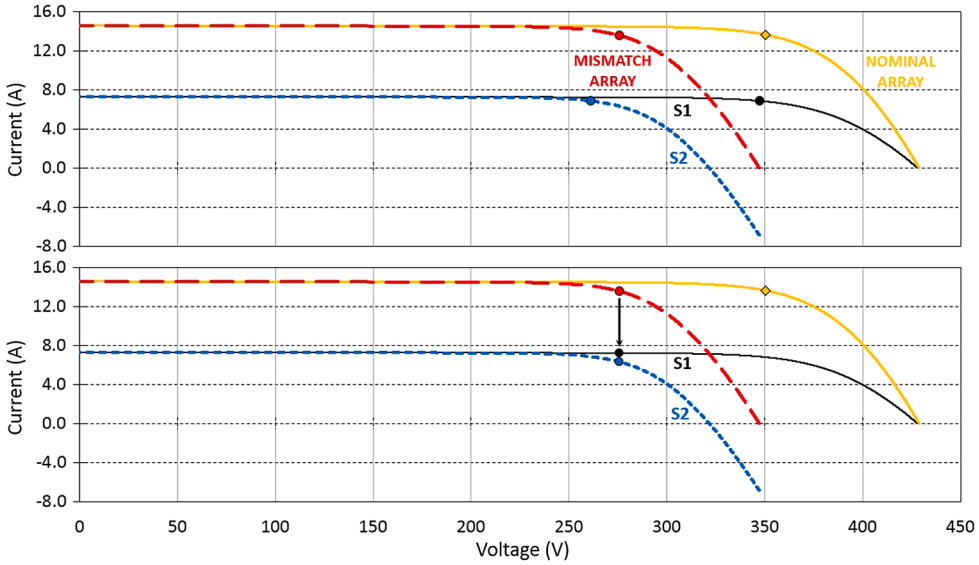

Fig. 7. Simulation of a 3-module mismatch without blocking diodes. a) the upper portion indicates the nominal array IV curve (solid yellow; for reference), the individual string IV curves for the nominal (solid black, S_1) and shortened (dashed blue, S_2) strings, and the mismatch array IV curve (dashed red). Maximum power points for each IV curve are indicated. b) the lower portion indicates the expected operating point of each string given the mismatch array maximum power point.

module level simulation. Using rough values for the additional array-level elements, the nominal array simulation over estimates the array V_{oc} by 3.9%; based on the module simulation, an over prediction of 2.76% is expected. V_{mpp} of the array is overestimated by the simulation by 8.2%; -0.12% is expected. Current parameters show similar non-additive errors which are partially explained by the simulation's error in predicting the key voltage parameters of the array. I_{mpp} is under-estimated by 1.2%. Several possibilities exist for the source of the error between simulation and experiment, including: 1) incorrect values for model parameters, 2) sensor error in the measurements of experimental data, specifically in string voltage, string current, or incident plane-of-array irradiance, or 3) an unanticipated issue in extending module element simulations to an array level.

Investigating the first potential source of error, a primary difference between the module model and the array model is the inclusion of cabling and string-end elements: blocking diodes, and home run cable and connector resistance. Removal of the blocking diodes from the simulation results in a minimal change for all mismatch conditions at the maximum power point, nominal through the six-module mismatch. The diode elements do not impact the simulation maximum power point results. However, alteration of the home run resistance parameter, R_{HR}, yields a substantial change in the simulation's maximum power point results. It is necessary to evaluate how a change in the R_{HR} parameter impacts the maximum power point simulation results across all mismatch conditions, and how experimental results compare to the simulations. The 6.2kW experimental PV array in the field was reconfigured over multiple weeks to obtain maximum power point (V_{MPP},I_{MPP}) and irradiance data corresponding to each of the desired mismatch cases. Operating point values were obtained by filtering the raw measurement data for stable sky and desired operating conditions of 800W/

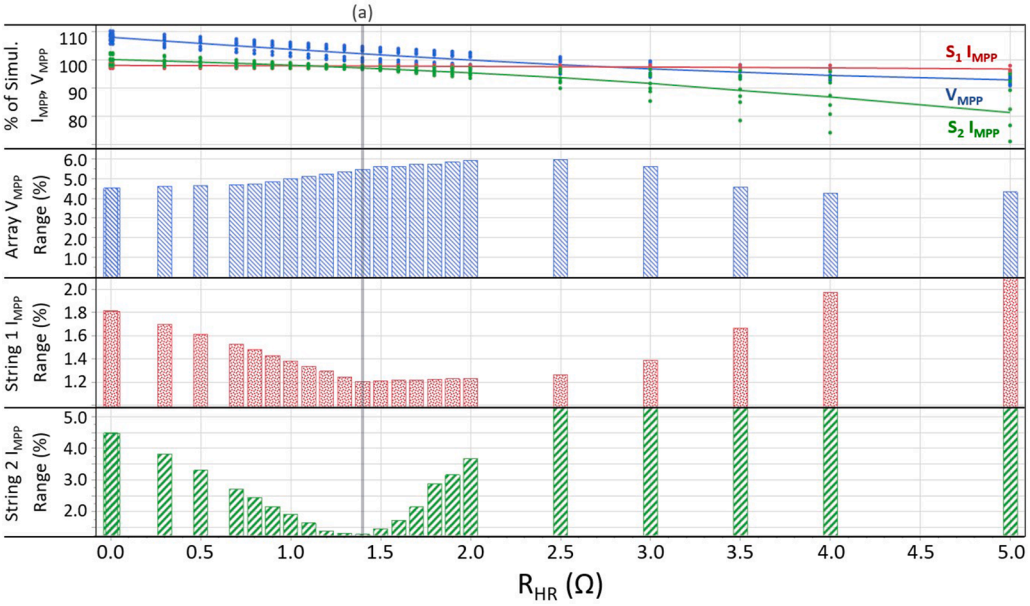

Fig. 8. Error between the simulation and experiment is minimized by adjusting the array-level R_{HR} resistance. Indicated at (a), the maximum power point current error is minimized at 1.4Ω.

m^2 and 50°C. Comparing the simulation value and experimentally determined value for each of the seven mismatch conditions yields a set of errors: a positive error indicating that the simulation overestimates the parameter, or a negative error indicating that the simulation underestimates the parameter. An ideal situation is one where the error is equivalent across all test conditions. This would indicate that the remaining error is systematic and may be accounted for by traditional measurement error in the experimental data.

Iterating through a range of values for the model parameter, it is possible to find a value for which the spread across the test conditions is minimized. Simulations were repeated for R_{HR} values in the 0-5Ω range and resulting maximum power point parameter values were compared with experimental data. Shown in Fig. 8, a change in this resistance has a substantial impact on the simulation results. A minimum range is identified at a value of 1.4Ω. Indicated in the figure at (a), the S_2 error is reduced to a range of 1.36%. Correspondingly, the S_1 error is reduced to 1.27%. It is worth emphasizing that these are ranges incorporating the nominal and all mismatch conditions. The V_{MPP} value does not achieve a minimum at this same value of resistance, but at 1.4Ω has a range of 5.26% across the seven conditions. Fig. 9(A) compares the maximum power point simulation results (open triangles) to experimentally determined values (solid diamonds) at 800W/m^2 and 50°C for each of the seven test conditions. As shown in Fig. 9(B) the error in V_{MPP} moves from a positive value (overestimate) to a negative value (underestimate) as the condition moves from nominal through the six module mismatch with an average overestimate of $+2.11 \pm 6.54\%$ (3σ). I_{MPP} for the nominal string (S_1) and test string (S_2) show an underestimate of the current through all test conditions at $-3.88 \pm 1.38\%$ (3σ) and $-4.62 \pm 1.52\%$ (3σ) respectively. By adjusting model parameter R_{HR}, the model can simulate a variety of mismatch conditions and achieve a consistent error from the experimental data set, an error which may be correctable.

The second potential source of error - sensor error in the measurements of experimental data, specifically in string voltage, string current, or incident plane-of-array irradiance - may be investigated now that a consistent underestimate of the I_{MPP} values is established. Sensor error may impact the error in multiple ways. For instance, current measurement devices may be out of calibration. In the case of the test array, two DC power meters are utilized, one for each string. The consistent error between the strings indicates that either the meters are uniformly out of calibration or the source of error may be in the irradiance measurement, a value which is used for filtering. If the irradiance sensor reads low by 2.59%, the average error in I_{MPP} for S_1 and S_2 and a value which is within reason for a photodiode pyranometer, then the actual irradiance may be 820.7W/m^2 and not the expected 800W/m^2. As a result, the measured current will be high by approximately 2.59% because current is fundamentally proportional to incident irradiance. In reality, there is likely a combination of meter and pyranometer errors contributing to the difference between simulation and experimental results. Because both ultimately impact the reported current, they may be pooled into a single correction factor of 0.9741 to the measured current which, when applied, results in a corrected version of Fig. 9: Fig. 10. After correction, I_{MPP} for the nominal string (S_1) and test string (S_2) show a reduced error between the simulation and experimental values through all test conditions at $+0.35 \pm 1.46\%$ (3σ) and $-0.36 \pm 1.58\%$ (3σ) respectively. Given the relatively low error between the corrected model and the experimental data, the model may be expanded to predict the impact on arrays of larger size and complexity as discussed in Section 4.

3.3. 6.2 kW PV plant simulation and model validation at V_{OC}

Commercial sites often parallel two or more strings at the input of each combiner. Often the series fuse located within the combiner is sized for the combined series fuse current of the paralleled strings to reduce the cost of fuses. For example, two strings that individually require a maximum 15A series fuse may be paralleled and protected as a group with a single 30A fuse. This poses a potential problem when strings are mismatched due to the removal of modules from any one or more strings within the array. Under normal conditions, and as detailed in Section 3.2, at the maximum power point all strings are contributing to the generation of the array. However, when the inverter is powered off for maintenance or due to a failure, the array is left in an open circuit condition with each string attempting to sit at V_{OC}. When a mismatch in the string length exists, neither the nominal length strings nor the shortened string are able to achieve the ideal condition of no current flow; a portion of the array has a net positive current flow and another portion has a net negative (reverse) current flow. This section explores simulation and experimental results both with and without blocking diodes when the array is maintained at open circuit; in all cases the two paralleled strings remain electrically connected at the inverter but the inverter is disconnected from the grid in standby mode.

Referencing Figs. 6 and 7 for the condition of a 3-module mismatch between S_1 and S_2, a significant difference is notable at open circuit. With blocking diodes, the shortened string is prevented from operating under a reverse current condition. The diodes allow the array to achieve the V_{OC} of the most significant string, in this case S_1. Above approximately 320V, S_2 generates no current and the array behaves as if composed of a single string. Conversely, without blocking diodes, above

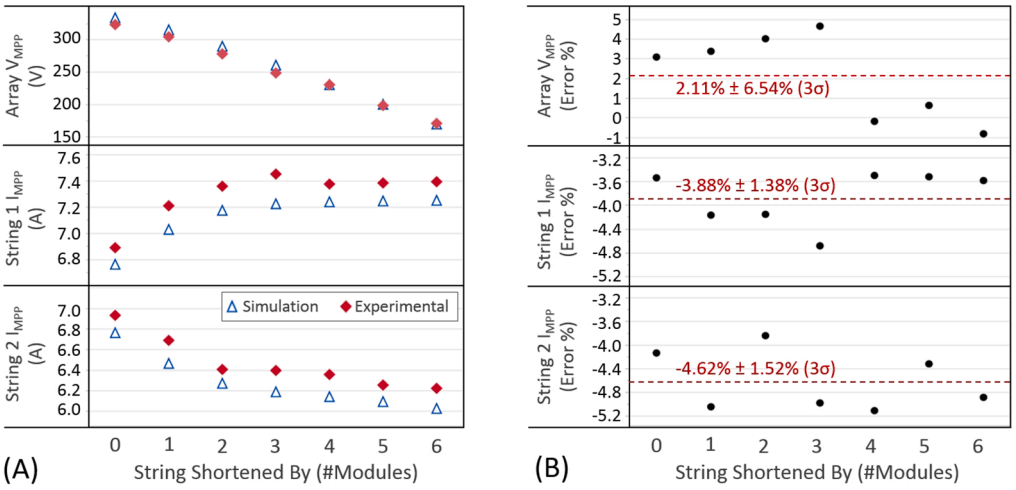

Fig. 9. Simulation and experimental maximum power point parameters at 800W/m^2 and 50°C for each of the seven test conditions presented in (A) engineering units, and (B) as the percent error from the experimental data..

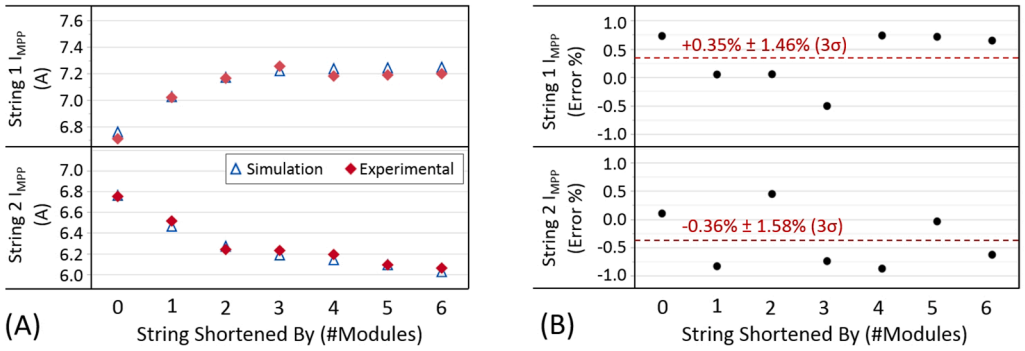

Fig. 10. Simulation and experimental maximum power point parameters at $800W/m^2$ and $50°C$ for each of the seven test conditions, corrected for current and irradiance measurement error by applying a correction factor of 0.9741 to the S_1 and S_2 I_{MPP} experimental data set. Results are presented in (A) engineering units, and (B) as the percent error from the experimental data..

the V_{OC} of S_2, S_1 forces current through S_2 and creates an unprotected current loop. As the voltage rises towards the V_{OC} of the mismatch array, the current increases until the current in the shortened string is equal and opposite to the current generated by S_1 at V_{OC}.

The first set of tests monitors the array and string behavior while the inverter is operating and connected to the electrical grid. This simulates normal operating conditions with a functional inverter and an array with mismatched string lengths. The second experiment simulates a maintenance condition where the inverter is manually disconnected from the grid, has failed, or is otherwise not managing the connected array during elevated irradiance conditions. The test array inverter is disconnected from the electrical grid for these experiments and is not influencing array operation; DC meters record the string voltage and current of the parallel connected strings. Experiments without blocking diodes are limited to the 1- through 3-module shortened conditions to limit the risk of excessive reverse current.

Simulations are run at irradiance levels between 5 and 1000W/m^2 to predict the behavior in S_1 and S_2 through the nominal and six mismatch conditions. The nominal case simulations predict that, throughout the full range of irradiance, the strings remain balanced with no current flow. However, as S_2 is shortened, the equilibrium point between the two strings decreases in voltage and therefore enables current flow between the nominal length string and the shortened string. As the level of mismatch increases, the maximum current flow at any given irradiance increases.

In the first test scenario, the inverter manages the mismatch array as normal. The transition between V_{OC} and maximum power point tracking both at sunrise and sunset across multiple days is of primary interest. The array is reconfigured for each mismatch condition and string-level metering (voltage, current) and photodiode pyranometer irradiance data is collected. Just above 0W/m^2, the array sits at the V_{OC} of the mismatch array with small positive and negative currents in S_1 and S_2 respectively. As irradiance increases, the array tends to deliver enough current to the inverter to enable maximum power point tracking above 30W/m^2, at which point the array operates near the expected V_{MPP} of the mismatch array. While tracking the maximum power point, the array operates the same as if there are blocking diodes present. Approaching sunset, the inverter tends to cease maximum power point tracking below about 20W/m^2 at which point the array again transitions to the V_{OC} of the mismatch array with small positive and negative currents in S_1 and S_2. In this scenario, reverse current is a concern only below approximately 30W/m^2 when the mismatch array sits at V_{OC}.

In the second scenario, the inverter is disabled so the mismatch array achieves equilibrium at the open circuit voltage. Data was collected for the 1-module mismatch condition between 0 and 1000W/m^2 and for the 2- and 3-module mismatch conditions up to a maximum irradiance of 325 and 450W/m^2 respectively. For all three test conditions, measured currents in S_2 are of opposite sign and approximately equal magnitude of the corresponding current generated by S_1. As the mismatch increases from one to three modules, the current level at a given irradiance increases. Fig. 11 incorporates both simulation and experimental results for the described scenarios. The simulation tends to underestimate the level of current generated by S_1 and therefore the corresponding level of reverse current consumed in S_2. For instance, at 325W/m^2, current is underestimated in both strings for the three test conditions, 1-module through 3-module respectively: S_1 (-18.3%, -9.3%, and -8.0%) and S_2 (-13.0%, -6.0%, and -5.1%). The error between the simulation and the experimental data decreases as the array mismatch increases. Although not without error, the trends predicted by the simulations are seen in the experimental data which allows these simulations to be used to model higher complexity arrays with the understanding that if the reverse current in the simulation exceeds the manufacturer stated current limits

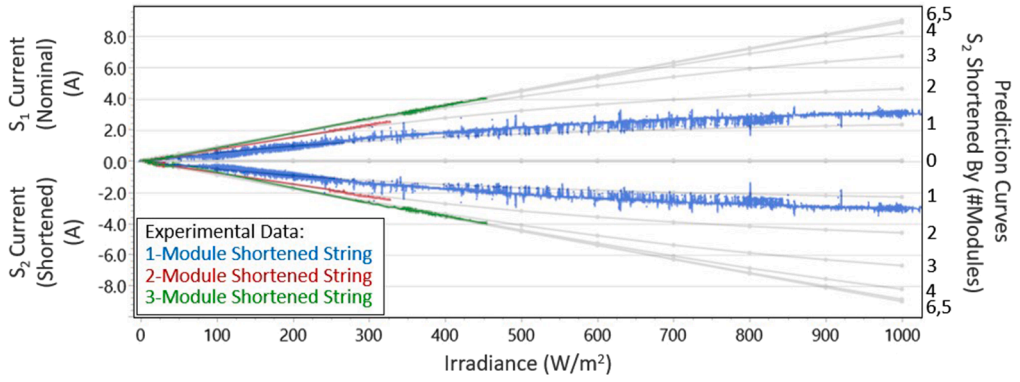

Fig. 11. Simulation and experimental data of the $6.2kW$ two-string array without blocking diodes at V_{OC}. Gray curves indicate simulation predictions. Colored points indicate measured data from the test array: blue for 1-module shortened, red for 2-module shortened, and green for 3-module shortened conditions..

within a module, it is probable that the predicted currents will be seen in the field.

4. Discussion

4.1. Mismatch analysis under MPPT conditions

Of primary concern to operators of photovoltaic plants is continual operation at the maximum power point, to the maximum extent possible. Removal of strings or sub-arrays because of required maintenance, annual inspection of modules, or repairs may result in a reduced potential output from the system. To limit the impact, some operators will shorten one or more strings within an array when a module needs to be removed; the inverter thus finds a new maximum power point for the mismatched array until the string lengths are returned to normal.

Simulations initially underestimated I_{MPP} and overestimated V_{MPP} when compared to experimental measured values. Investigation of potential sources of error leads to a empirical method for refining the value of the additional model resistive element R_{HR}, and an adjustment to the measured current to correct for a potential miscalibration of the photodiode pyranometer. As a result, the overall error in I_{MPP} for the nominal string (S_1) and test string (S_2) between the simulation and experimental values, through all test conditions, reduces to $+0.35 \pm 1.46\%$ (3σ) and $-0.36 \pm 1.58\%$ (3σ) respectively.

Comparisons between P_{MAX} and V_{MPP} for the nominal and test conditions is shown in Table 3. Removal of a single module from S_2 results in a drop in P_{MAX} of 260.8W, a power reduction equivalent to 129% of the rated NOCT power of the module, or 1.29 equivalent modules. The reduction in P_{MAX} of the array exceeds the contribution of the removed module. As the mismatch increases, the maximum power point power reduction increases non-linearly with the level of mismatch. Similarly, the reduction in V_{MPP} increases as the level of mismatch increases. With a 1-module mismatch, V_{MPP} of the array drops by 18.6V. A 2-module mismatch reduces V_{MPP} by 44V, or 22V per module. The most extreme simulation indicates a V_{MPP} reduction of 163.8V, or 27.3V per module. The presence or absence of string-end blocking diodes does not impact the simulations at the maximum power point to any significant degree; this is supported by the experimental data, which shows no discernible difference in measurements for the 1- through 3-module mismatch conditions with and without blocking diodes, Fig. 12.

The authors expect that strings of shorter or longer lengths than the one studied (12-module strings), higher complexity arrays, and those with substantially more paralleled strings may experience a different reduction in P_{MAX} beyond the summed power of the removed modules. Multiple mismatched strings within the same array or sub-array may be impacted differently than predicted with the simple test case presented in this work. It is worth noting that a significant mismatch also has the potential to move the maximum power point to a voltage below the operating range of the inverter or, in extreme cases, may shift the global maximum power point. Future modeling efforts to explore more complex scenarios is anticipated.

Table 3
Simulation conditions and predicted maximum power point operation at 800W/m^2 and 50°C for the two string, grid-tied 6.2kW experiment array at the UCF FSEC test field in Cocoa, Florida. The right column is the power reduction from the nominal array condition at P_{MAX} in units of equivalent modules at NOCT (202W).

Condition	I_{MPP} (A)	V_{MPP} (V)	P_{MPP} (W)	P_{MAX} Reduction (Equivalent Modules)
Nominal	13.52	333.2	4504.4	0
1-Module Shortened	13.49	314.6	4243.6	1.29
2-Module Shortened	13.44	289.2	3886.2	3.06
3-Module Shortened	13.41	260.1	3486.8	5.04
4-Module Shortened	13.37	230.0	3076.1	7.07
5-Module Shortened	13.33	199.7	2662.9	9.12
6-Module Shortened	13.27	169.4	2248.6	11.17

4.2. Mismatch analysis under V_{OC} conditions

The presented work is limited to a two string mismatch array. However, the trends displayed through simulation and supported by experiment expose potential design concerns for larger systems which may, at times, operate with shortened strings for maintenance or other purposes. These larger arrays are not usually designed with or operate with string-end blocking diodes.

Under operation at the maximum power point, the shortened strings will impact the operating point of the array and reduce the potential power output of the system as discussed in the preceding section; this is a concern from a power production standpoint. When in a standby condition, such as low-irradiance times near sunrise and sunset, the inverter will not control the array and therefore the mismatched array will maintain a self-regulating open circuit condition wherein the current will flow from the nominal length strings through the shortened strings such that the overall current balance between the strings is maintained. Similarly, an open circuit condition exists when the inverter is taken offline for maintenance, typically during daylight hours. This is the more extreme of the two discussed open circuit conditions because the potential reverse current through the shortened string is a function of the incident irradiance and number of paralleled strings.

V_{OC} experiments were restricted up to a 3-module mismatch. Simulations underestimated the level of current flow through both the nominal and shortened strings. Even so, extrapolation of the mismatch conditions to 1000W/m^2 at 50°C suggests that even in the smallest of mismatched string arrays (two strings), the reverse current may exceed three amperes for a 1-module shortened string mismatch up to approximately seven amperes for a 3-module shortened string mismatch. It is unclear, however, if reverse currents in practice will exceed the manufacturer specified reverse current limit or, in the absence of a stated reverse current limit, the series fuse rating.

An expansion of the simulations discussed in Section 3 provides an initial view into the stated concern. By expanding the total number of paralleled strings and maintaining a single shortened string, the simulated array expands from two total strings to 24. Three mismatch conditions were simulated and consisted of a 1-, 3-, and 5-module shortened mismatch string. Fig. 13 describes the simulated reverse currents in the shortened string. A mismatch string shortened by a single module will experience a reverse current that approaches 5A. The simulations are not extensive enough to determine if the reverse current is asymptotic at a certain current or if this will continue to increase as the number of paralleled strings increases. Increasing the level of mismatch in the shortened string increases the reverse current: a 3-module shortened string approaches the series fuse rating threshold of 15A with eight paralleled strings; a 5-module shortened string exceeds 15A with three paralleled strings. Defining which array configurations could exceed reverse current limits will be explored in future work.

4.3. Additional considerations

Although not discussed in the present work, the authors acknowledge that there are expected thermal impacts to the nominal and shortened strings within a mismatch array that should manifest as changes to operating temperature, both at the cell level and at the module level. Infrared imaging should reveal these changes at a macroscopic level, but a more detailed theoretical analysis is necessary.

5. Conclusions

The present work utilizes a simple modeling and validation technique to explore the impacts of mismatched strings on the performance of a photovoltaic array. The present study has investigated and quantified shortened string mismatch losses for 12-module strings; mismatch

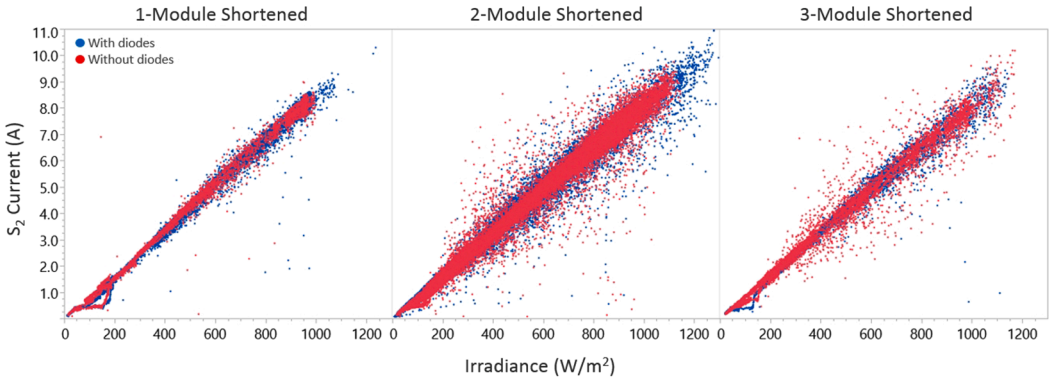

Fig. 12. Measured S_2 currents at maximum power point for the 1- through 3-module shortened string conditions as a function of incident irradiance. Blue dots represent the condition with diodes and red dots are without diodes.

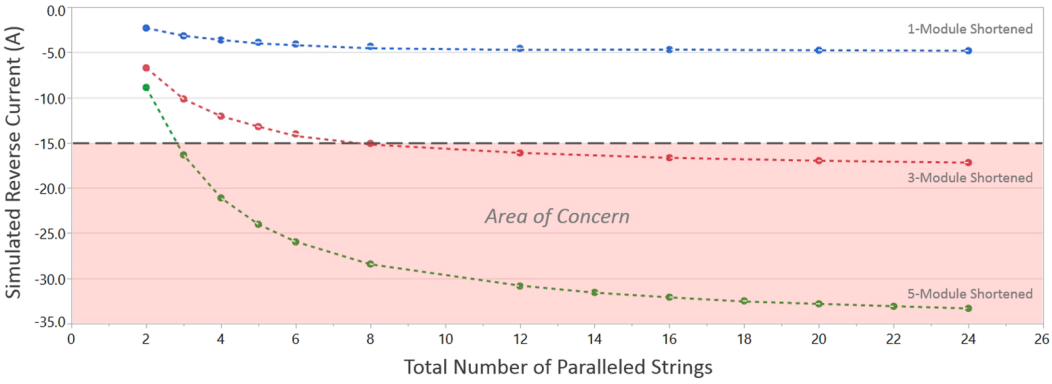

Fig. 13. Simulation of multi-string arrays consisting of up to 24 total strings with a single shortened mismatch string. Colored points indicate simulation results for the mismatch string reverse current: blue for 1-module shortened, red for 3-module shortened, and green for 5-module shortened conditions. The red shaded area indicates the area of concern for exceeding the series fuse rating of the modules used in this work.

losses in shorter or longer strings may differ from the present study and warrants further investigation. Simulations are refined and supported with experimental data for the nominal condition of equal-length strings as well as for unequal-length strings shortened by one to six modules, both with and without the use of string-end blocking diodes. Modeling of PV systems are valuable tools to study mismatch qualitatively. However, proper tuning of the model is necessary to reduce the model error when modeling a specific PV system. The technique used to refine the simulations and match experimental behavior may be applied to other modules and array configurations.

Operation at the array maximum power point is discussed with the noted impact of a reduction in V_{MPP} and P_{MAX}, which increases non-linearly with an increasing level of mismatch. Resulting power loss is greater than the power contribution of the removed modules alone. For example, a string shortened by one module results in a 1.29 module equivalent power loss, and shortening by six modules results in an 11.17 module equivalent power loss. Simulation and experimental studies both proved that blocking diodes prevent power losses due to string length mismatch under these conditions and that operation at V_{MPP} is not substantially impacted by the presence or absence of blocking diodes.

Under open circuit conditions, such as low-irradiance conditions or when the inverter is in standby, the shortened string is placed in reverse current to a level that balances with the current generation from the nominal length parallel strings. Concerns are raised about the potential for the level of reverse current to exceed the rating of the modules. Based on the presented work, PV arrays at V_{OC} can tolerate at most one missing module per string without exceeding the series fuse rating due to over current because the reverse current will likely never be larger than about 5 amperes no matter the number of strings in parallel. However, that may be enough to create severe hotspots and damage a module, thus leading to more significant mismatch conditions and potentially higher reverse currents.

CRediT authorship contribution statement

Ryan M. Smith: Methodology, Investigation, Software, Formal analysis, Visualization, Writing - original draft, Writing - review & editing. **Manjunath Matam:** Methodology, Investigation, Writing - original draft, Writing - review & editing. **Hubert Seigneur:** Funding acquisition, Project administration, Supervision, Methodology, Writing - original draft, Writing - review & editing.

Declaration of Competing Interest

The authors declare that they have no known competing financial interests or personal relationships that could have appeared to influence the work reported in this paper.

Acknowledgements

This material is based upon work funded by the U.S. Department of Energy's Solar Energy Technologies Office Award Number DE-EE0008157. The opinions, findings, and conclusions stated herein are those of the authors and do not necessarily reflect those of the U.S. Department of Energy.

References

[1] International Energy Agency, Renewables 2020, 2021. https://www.iea.org/reports/renewables-2020.

[2] U.S. Energy Information Administration, Levelized costs of new generation resources in the annual energy outlook 2021, 2021. https://www.eia.gov/outlooks/aeo/.

[3] Lillo-Bravo I, González-Martínez P, Larrañeta M, Guasumba-Codena J. Impact of energy losses due to failures on photovoltaic plant energy balance. Energies 2018;11. https://doi.org/10.3390/en11020363. https://www.mdpi.com/1996-1073/11/2/363.

[4] N.M. Kumar, S. Dasari, J.B. Reddy, Availability factor of a pv power plant: evaluation based on generation and inverter running periods, Energy Procedia 147 (2018) 71–77. https://www.sciencedirect.com/science/article/pii/S1876610218301917. https://doi.org/10.1016/j.egypro.2018.07.035, international Scientific Conference Environmental and Climate Technologies, CONECT 2018, 16-18 May 2018, Riga, Latvia.

[5] Ilse K, Micheli L, Figgis BW, Lange K, Daßler D, Hanifi H, Wolfertstetter F, Naumann V, Hagendorf C, Gottschalg R, Bagdahn J. Techno-economic assessment of soiling losses and mitigation strategies for solar power generation. Joule 2019;3:2303–21. https://doi.org/10.1016/j.joule.2019.08.019. https://www.sciencedirect.com/science/article/pii/S2542435119304222.

[6] Shin WG, Lim JR, Kang GH, Ju YC, Hwang HM, Ko SW. Current flow analysis of pv arrays under voltage mismatch conditions and an inverter failure. Appl Sci 2019;9. https://doi.org/10.3390/app9235163. https://www.mdpi.com/2076-3417/9/23/5163.

[7] Liu G, Yu W, Zhu L. Experiment-based supervised learning approach toward condition monitoring of pv array mismatch. IET Generation, Trans Distrib 2019;13:1014–24. https://doi.org/10.1049/iet-gtd.2018.5164.

[8] Manganiello P, Balato M, Vitelli M. A survey on mismatching and aging of pv modules: The closed loop. IEEE Trans Ind Electron 2015;62:7276–86. https://doi.org/10.1109/tie.2015.2418731.

[9] Bastidas J, Franco E, Petrone G, Ramos-Paja C, Spagnuolo G. A model of photovoltaic fields in mismatching conditions featuring an improved calculation speed. Electric Power Systems Res 2013;96:81–90. https://doi.org/10.1016/j.epsr.2012.10.020.

[10] Orozco-Gutierrez M, Ramirez-Scarpetta J, Spagnuolo G, Ramos-Paja C. A technique for mismatched pv array simulation. Renewable Energy 2013;55:417–27. https://doi.org/10.1016/j.renene.2013.01.009.

[11] Mahmoud Y, El-Saadany EF. Enhanced reconfiguration method for reducing mismatch losses in PV systems. IEEE J Photovoltaics 2017;7:1746–54. https://doi.org/10.1109/jphotov.2017.2752708.

[12] Potnuru SR, Pattabiraman D, Ganesan SI, Chilakapati N. Positioning of PV panels for reduction in line losses and mismatch losses in PV array. Renewable Energy 2015;78:264–75. https://doi.org/10.1016/j.renene.2014.12.055.

[13] Lappalainen K, Valkealahti S. Effects of irradiance transition characteristics on the mismatch losses of different electrical PV array configurations. IET Renewable Power Generation 2017;11:248–54. https://doi.org/10.1049/iet-rpg.2016.0590.

[14] Orozco-Gutierrez ML, Spagnuolo G, Ramirez-Scarpetta JM, Petrone G, Ramos-Paja CA. Optimized configuration of mismatched photovoltaic arrays. IEEE J Photovolt 2016;6:1210–20. https://doi.org/10.1109/jphotov.2016.2581481.

[15] Olalla C, Deline C, Clement D, Levron Y, Rodriguez M, Maksimovic D. Performance of power-limited differential power processing architectures in mismatched PV systems. IEEE Trans Power Electron 2015;30:618–31. https://doi.org/10.1109/tpel.2014.2312980.

[16] Ji Y-H, Jung D-Y, Kim J-G, Kim J-H, Lee T-W, Won C-Y. A real maximum power point tracking method for mismatching compensation in PV array under partially shaded conditions. IEEE Trans Power Electron 2011;26:1001–9. https://doi.org/10.1109/tpel.2010.2089537.

[17] Pillai DS, Ram JP, Rajasekar N, Mahmud A, Yang Y, Blaabjerg F. Extended analysis on line-line and line-ground faults in pv arrays and a compatibility study on latest nec protection standards. Energy Conversion Management 2019;196:988–1001. https://doi.org/10.1016/j.enconman.2019.06.042.

[18] Satpathy PR, Sharma R. Power and mismatch losses mitigation by a fixed electrical reconfiguration technique for partially shaded photovoltaic arrays. Energy Conversion Management 2019;192:52–70. https://doi.org/10.1016/j.enconman.2019.04.039.

[19] Chaudhari C, Kimball GM, Hickey R, Bourne B. Quantification of system-level mismatch losses using pvmismatch. In: 2018 IEEE 7th World Conference on Photovoltaic Energy Conversion (WCPEC) (A Joint Conference of 45th IEEE PVSC, 28th PVSection 34th EU PVSEC); 2018. p. 3626–9. https://doi.org/10.1109/PVSC.2018.8548107.

[20] Mansur AA, Amin MR, Islam KK. Performance comparison of mismatch power loss minimization techniques in series-parallel pv array configurations. Energies 2019;12. https://doi.org/10.3390/en12050874. https://www.mdpi.com/1996-1073/12/5/874.

[21] S.K. Sahoo, M. Shah, N.A. Dawlatzai, R. Ann Jerin Amalorpavaraj, Assessment of mismatching in series and parallel connection of the pv modules of different technologies and electrical parameters (2020) 1–5.

[22] Wang Z, Zhou N, Gong L, Jiang M. Quantitative estimation of mismatch losses in photovoltaic arrays under partial shading conditions. Optik 2020;203:163950.

[23] Deline C, Ayala Pelaez S, MacAlpine S, Olalla C. Estimating and parameterizing mismatch power loss in bifacial photovoltaic systems. Progress Photovoltaics: Res Appl 2020;28:691–703. https://doi.org/10.1002/pip.3259.

[24] Wang H, Cheng X, Yang H, He W, Chen Z, Xu L, Song D. Potential-induced degradation: Recombination behavior, temperature coefficients and mismatch losses in crystalline silicon photovoltaic power plant. Solar Energy 2019;188:258–64.

[25] Shin WG, Lim JR, Kang GH, Ju YC, Hwang HM, Ko SW. Current flow analysis of PV arrays under voltage mismatch conditions and an inverter failure. Appl Sci 2019;9. https://doi.org/10.3390/app9235163.

[26] Lee CG, Shin WG, Lim JR, Kang GH, Ju YC, Hwang HM, Chang HS, Ko SW. Analysis of electrical and thermal characteristics of pv array under mismatching conditions caused by partial shading and short circuit failure of bypass diodes. Energy 2021;218:119480.

[27] Ishii T, Choi S, Sato R, Chiba Y, Masuda A. Potential-induced degradation in photovoltaic modules composed of interdigitated back contact solar cells in photovoltaic systems under actual operating conditions. Progress Photovoltaics: Res Appl 2020;28:1322–32. https://doi.org/10.1002/pip.3329.

[28] M. Sengupta, A. Habte, C. Gueymard, S. Wilbert, D. Renné, T. Stoffel, Best practices handbook for the collection and use of solar resource data for solar energy applications, 2017. https://www.nrel.gov/docs/fy18osti/68886.pdf. 10.2172/1411856.

[29] National Renewable Energy Laboratory, Sandia National Laboratory, SunSpec Alliance, and the SunShot National Laboratory Multiyear Partnership (SuNLaMP) PV O&M Best Practices Working Group, Best practices for operation and maintenance of photovoltaic and energy storage systems, 2018. https://www.nrel.gov/docs/fy19osti/73822.pdf. DOI: 10.2172/1489002.

[30] D. Fregosi, C. Libby, M. Smith, M. Bolen, Guidance on pv module replacement, in: 2020 47th IEEE Photovoltaic Specialists Conference (PVSC), 2020, pp. 1581–1583. DOI: 10.1109/PVSC45281.2020.9300867.

[31] Wurster TS, Schubert MB. Mismatch loss in photovoltaic systems. Solar Energy 2014;105:505–11. https://doi.org/10.1016/j.solener.2014.04.014.

[32] Vargas J, Goss B, Gottschalg R. Large scale pv systems under non-uniform and fault conditions. Solar Energy 2015;116:303–13. https://doi.org/10.1016/j.solener.2015.03.041. https://www.sciencedirect.com/science/article/pii/S0038092X15001681.

[33] Jinko Solar, Eagle 60 Datasheet, 2015. https://y19jx2zo8mb2zyqyo1njsh26-wpengine.netdna-ssl.com/ wp-content/uploads/2019/03/US-Eagle-60-255-270w.pdf.

[34] Analog Devices, LTspice Simulator, 2021. https://www.analog.com.

[35] Cubas J, Pindado S, Manuel CD. Explicit expressions for solar panel equivalent circuit parameters based on analytical formulation and the lambert W-function. In: Proceedings of 1st International e-Conference on Energies; 2014. https://doi.org/10.3390/ece-1-c013.